Computations of the HDR thermal mixing experiments and analysis of mixing phenomena

W.Häfner, K.Fischer & L.Wolf
Battelle-Institut e.V., Frankfurt am Main, FR Germany

1. ABSTRACT

The calculations presented in the following were performed within the analytical part of the German HDR research programme into mixing phenomena during the high pressure injection phase.
For a selected experiment, pre-test calculations with the code SOLA-PTS are presented and discussed in comparison with the experimental data. The data were used also for a detailed analysis of mixing phenomena near the injection nozzle. The governing parameters identified in this analysis, and the physical models based on them are presented and discussed. Finally, suggestions for improvements of an existing physical model are made, taking into account available international experimental data.

2. INTRODUCTION

Thermal stratification in the cold leg of a PWR may lead to pressurized thermal shock (PTS). This may occur during the high pressure injection (HPI) of cold emergency core coolant water under low or stagnant loop flow conditions.
The mixing characteristics govern the temperature transient which controls the evaluation of thermal stress in the cold leg and vessel wall. To resolve the PTS issue, both U.S.NRC and EPRI performed a large number of experiments in scaled reactor cold leg and downcomer facilities /1-3/.
In addition to this experimental research, great analytical efforts were undertaken to develop complex computer codes /4/. Beside these rather expensive tools, fast, inexpensive codes /3/ and engineering models /5,6/ have been developed and verified with the help of the scaled experiments, since such models require correlations to describe the governing physical phenomena. Since the entrainment correlation has been developed by Oh et al. in 1983 to describe the mixing efficiency in the injection region as the most important mechanism, several additional thermal mixing experiments have been performed /7-10/. This enlarged data base from widely different facilities requires a re-examination and possibly a modification of the correlation.

3. HDR FACILITY AND TEST CONDITIONS

In contrast to most other test facilities, the HDR as shown in fig. 1 does not compare to real plants with a strict geometrical similarity /11/. On the other hand, this facility offers a number of advantages:

1) Complete 360° three-dimensional downcomer
2) Realistic density difference due to system press. of 11 MPa
3) Participating heat conducting structures
4) Correct thermal boundary conditions at the core barrel side of the downcomer
5) Correct connection of the downcomer to the lower plenum
6) Realistic initial axial temp. gradients can be obtained
7) Structural and fracture mechanics studies are possible
8) Stationary as well as transient supply cond. may be simulated

During Phase II of the HDR Safety Programme, a total of 26 thermal mixing experiments were performed with three different HPI-nozzle arrangements and with a wide range of Froude numbers. Finite loop flow as well as stagnant loop conditions were investigated.

4. SOLA-PTS CALCULATIONS

The computer code SOLA-PTS was developed at the Los Alamos National Laboratory /4/ to simulate transient three-dimensional flow situations where buoyancy effects have a significant influence. This finite-difference code contains two different turbulence models and offers the option to also calculate the heat transfer between fluid and wall structure. Since cartesian coordinates are applied, the nodalization scheme shown in fig. 2 was used to simulate the HDR-TEMB facility in this model, a total of about 7000 nodes are used. Out of the series of pretest calculations performed with SOLA-PTS, experiment T32.41 is selected to give an idea of the predictive capabilities of the code. T32.41 was performed with an initial temperature of 300 °C, an injection temperature of 16 °C, a Froude number Fr_{CL} = 0,073 and stagnant loop conditions.

5. RESULTS OF CALCULATION AND COMPARISON WITH THE EXPERIMENT

The calculation was performed for a time period of 100 secs. Fig. 3 depicts the temperature distribution in the cold leg 10 sec after injection initiation using contour lines. The temperature in the downcomer and the upper part of the cold leg is unchanged and corresponds to the initial temperature of 300 °C.
At this time the cold front has advanced about halfway from the nozzle to the downcomer. Due to the violent mixing, the temperature increased from 20 °C to about 200 °C in the cold layer. To illustrate the velocity distribution at the same time point, fig. 4 shows the calculated velocities depicted by vectors. The most important features of the flow behaviour are the circulating currents in the region of the mixing layer resulting from natural

convection and the very low and uniform velocities in the remainder of the cold leg. The counter-current flow in the upper, hot part of the cold leg leads to a stabilization of a steep thermal gradient across the pipe.
Figures 5 and 6 depict the quasi-stationary state of the fluid flow during the injection, showing the fully established temperature stratification in the cold leg (fig. 5), and the nearly constant temperature outside the cold water plume in the plane of the downcomer (fig. 6) whereas inside the plume very strong temperature gradients occur as indicated by the closely spaced contour lines.
Figs. 7 through 11 show the comparison between pre-test calculation by SOLA-PTS and measured data at different positions or at different times. As indicated in fig. 7, the mixing in the injection area is predicted perfectly, as well as the stratification in the cold leg (as shown in fig. 8). However, the calculation gives a transport delay versus the data for positions further downstream of the injection. Due to the fact that, for realistic prediction of the flow velocity, many local conditions as the interlayer shear stress, the velocity profiles in the layers, the inclination angle of the interface etc. have to be considered, the agreement is still acceptable, since the chosen grid was too coarse to give these details. Important, however, for the assessment of SOLA-PTS is the excellent agreement with the measured initial temperature gradients at all positions. In the downcomer, 200 mm below the cold leg entrance (Z = 8650 mm) the temperature is predicted rather well as shown in fig. 9, but the calculated mixing in this region is overestimated, as compared to a position 450 mm below. Like in the injection area, a violent mixing with surrounding hot water takes place also in this inflow region. Due to the rather coarse nodalization these local effects could not be simulated by SOLA-PTS. This overestimation of mixing is clearly obvious from the comparison between fig. 10 and fig. 11 where the measured and calculated temperature distributions in the downcomer are shown (data and predictions fitted to a least-square surface).
Forthcoming post-test calculations will incorporate recommendations deduced from the above comparisons.

6. CORRELATION FOR DESCRIPTION OF THE MIXING IN THE INJECTION AREA

Alrealy the early experiments indicated that the most significant mixing occurs in the neighbourhood of the HPI-jet as result of the entrainment of counter-flowing hot water from the downcomer. For this entrainment, dimensionless correlations have been developed by Sun and Oh as well as by Theofanous. Generally speaking, both correlations show roughly the same functional dependencies. The important parameters governing the entrainment are the jet Froude-number Fr_{HPI} and the HPI jet travel lenght (L/d), where d is the nozzle diameter. Sun and Oh suggested the following function for the entrainment :

$$\varepsilon = 0.589\, \eta_{oh} - 0.796 \qquad \text{for } 1.5 \leq \eta \leq 13.8 \qquad (1)$$

with $\eta_{oh} = (L/d)\,(Fr_{HPI})^{-0.666}$

The jet length L is the distance between nozzle and the point where the jet touches the cold leg bottom. In the correlation of Theofanous, only the part of the jet surrounded by hot fluid h_H is considered as geometrical parameter:

$$\varepsilon = 0.5167 \quad \eta_{theo} \qquad (2)$$

with $\eta = (h_H/d)^{1.236} \; (Fr_{HPI})^{-0.414}$

Both correlations have been compared to the HDR-TEMB experiments, which have been performed under stagnant system conditions. For those experiments with HPI injection from the side the shorter contact length between jet and hot fluid have been accounted for. Figs. 12 and 13 show the comparison between the HDR data and predictions based on both correlations. As can be seen, the data are better represented by the correlation (1). A modification of the original Sun-Oh-correlation may already lead to an improvement. This is shown in fig. 14, where the exponent of Fr_{HPI} has been changed from 0.666 to 0.39 with a least square fit. For the HDR-data this change leads to a better agreement. But the range of η_{oh} is rather narrow. By considering all available data from the different test facilities, the parameters which have been found by a least-square fit do not differ very much from the original ones as indicated by fig. 15.
The model parameters shown in fig. 15 are based on the data from 5 widely different facilities. The IVO data are obtained even from a facility with cold water injection through a bottom nozzle into the cold leg. Therefore the mixing behavior of this special injection arrangement had been studied before so that the data from this test series were selected, where the same mechanism controls the mixing. Fig. 16 shows the entrainment coefficient versus the global Froude number. At low Fr_{CL}, perfect stratification takes place without vertical plume mixing. Here, the entraimnent is limited and increases with increasing injection flow rate. At the maximum, the counter current-flooding limit is reached and further increase of HPI flow leads to a decrease of hot water transport back from the downcomer and hence to a decrease of mixing.

Since the entrainment for top injection shows the same functional dependency as depicted in fig. 16 for Froude-numbers greater than 0.04 only data points with sufficiently large Froude-numbers (denoted by triangles) are selected to compare with the original function (1). As fig. 17 shows, the general trend of function (1) (solid line) and data (trialgular points) agree well, however, the observed mixing is somewhat stronger. Therefore, the mixing length for this experimental geometry with bottom injection must be adjusted by a geometry factor of about 1.6 to account for the longer HPI jet path. With this geometry factor, the IVO experimental data can be incorporated into the data base to improve the entrainment correlation. The modifications are not fundamentally; they reflect rather the enlargement of the data base. This result verifies the validity of the functional dependencies of the considered mixing model developed by Sun and Oh.

NOMENCLATURE

A = Cross-section area
d = Diameter
Fr = Froude-number
g = Gravitational acceleration
m = Mass flow rate
ρ = Density

$$Fr_{CL} = \frac{\dot{m}_{HPI} / (A_{CL}\,\rho_{HPI})}{\sqrt{g\,d_{CL}\,(\rho_{HPI} - \rho_{CL}) / \rho_{HPI}}}$$

$$Fr_{HPI} = \frac{\dot{m}_{HPI} / (A_{HPI}\,\rho_{HPI})}{\sqrt{g\,d_{HPI}\,(\rho_{HPI} - \rho_{CL}) / \rho_{HPI}}}$$

$$\varepsilon = \frac{\dot{m}_{entr}}{\dot{m}_{HPI}} = \frac{T_{mix} - T_{HPI}}{T_{CL} - T_{mix}}$$

REFERENCES

/1/ Fanning, M.W.; Rothe, P.H.: Transient Cooldown in a Model Cold Leg and Downcomer, EPRI NP-3118, 1983

/2/ Hashemi, A.; Goodman, J.: Thermal Mixing in a Rectangular Geometry Model of a Cold Leg With High Pressure Injection and a Downcomer, EPRI NP-2924, 1983

/3/ Theofanous, T.G. et al: Decay of Buoyancy Driven Stratified Layers with Applications to PTS, NUREG/CR-3700

/4/ Daly, B., et al.: SOLA-PTS: A Transient, Three-Dimensional Algorithm for Fluid-Thermal Mixing and Wall Heat Transfer in Complex Geometries, NUREG/CR-3822, 84

/5/ Oh, S.; Sursock, J.P.; Sun, K.H.: A Mixing Model for Transient Cooldown in a Reactor Cold Leg and Downcomer Under Stagnant Loop Flow, ASME-Paper No. 83-HT-13

/6/ Kim, J.H.: An Analytical Mixing Model for Buoyant Jet Injected into Pipe Flow, ASME-Paper No. 83-WA/HT-42

/7/ Dolan, F.X.; Valenzula, J.A.: Thermal and Fluid Mixing in a 1/2-Scale Test Facility, EPRI NP-3802, 1985

/8/ Giot, M.; Hernalsteen, P.; Stubbe, E.: Pressurized Thermal Shock-Mixing of a Direct Safety Injection Flow in a PWR Reactor Vessel Downcomer-Experimental and Analytical Results, Trans. 8th Intl. Conf. SMIRT, Brussels, Belgium, pp. 367-374 (paper F1G 1/2*)

/9/ Tuomisto, H.; Hytönen, Y.; Mustonen, P.: Two-Fifths Scale Thermal Mixing Test in a Semiannular Downcomer and Cold Legs, Proc. Intl. ANS/ENS Topical Mtg. on Thermal Reactor Safety, San Diego, CA, USA, 1986

/10/ Yoshimura, S. et al: Mixing Behaviour of Safety Injection Water Within the Cold Leg and the Downcomer Under Postulated Accidents, Proc. 3rd Intl. Top. Mtg. on Reactor Thermal Hydraulics, Newport, RI, USA, 1985

/11/ Wolf, L.; Schygulla, U.: Design Report: Thermal Mixing Experiments in Cold Leg and Downcomer, HDR-Test Group TEMB, T32, PHDR-Working Report No. 3.430/84, 85

/12/ Sun, K.M.; Oh, S.: A Correlation for Entrainment of Water in a Reactor Cold Leg by Coolant Injection under Stagnant Loop Flow, ASME; Paper No. 83-WA/HT-39

/13/ Wolf, L.; Schygulla,U.; Häfner, W.; Fischer, K.; Baumann, W.: Results of Thermal Mixing Tests at the HDR-Facility and Comparisons with Best-Estimate and Simple Codes, Proc. Third Intl. Top. Mtg. on Reactor Thermal Hydraulics, Newport, Rhode Island, USA, 85, paper 8. E

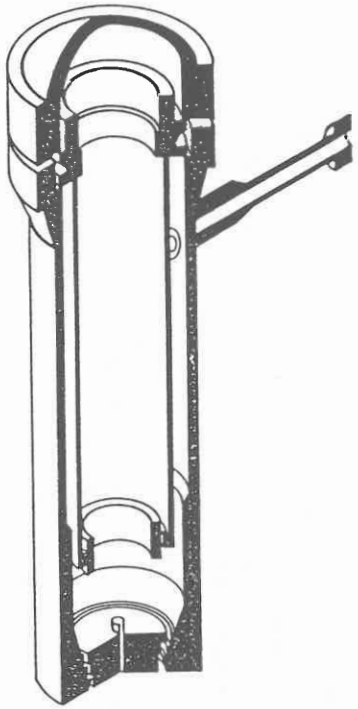

Fig. 1: HDR Pressure Vessel

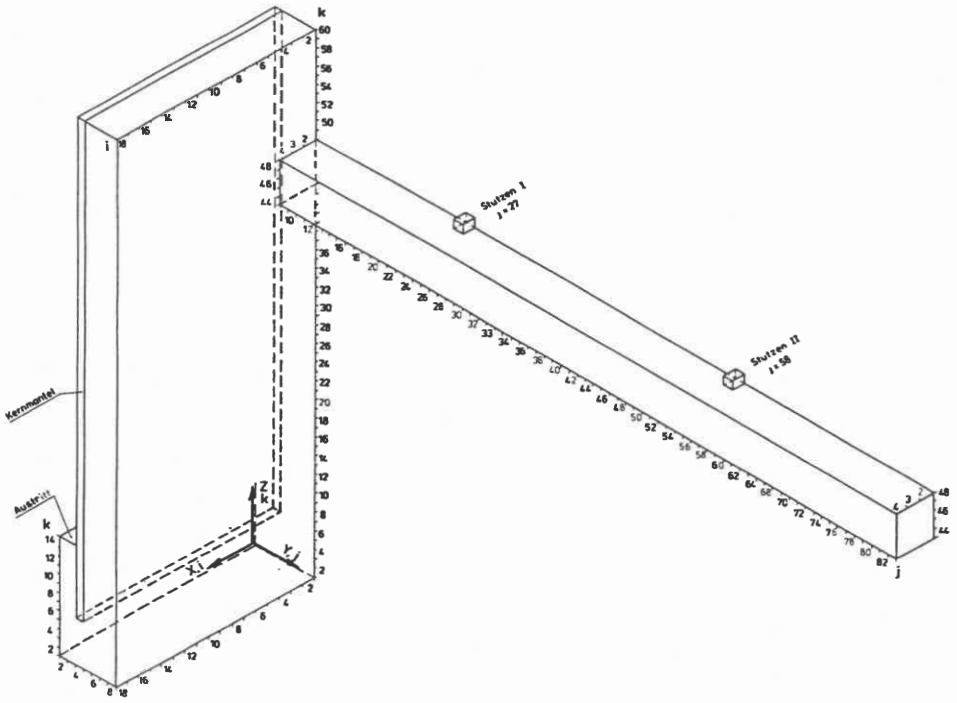

Fig. 2: SOLA-PTS Calculation Model and Nodalization

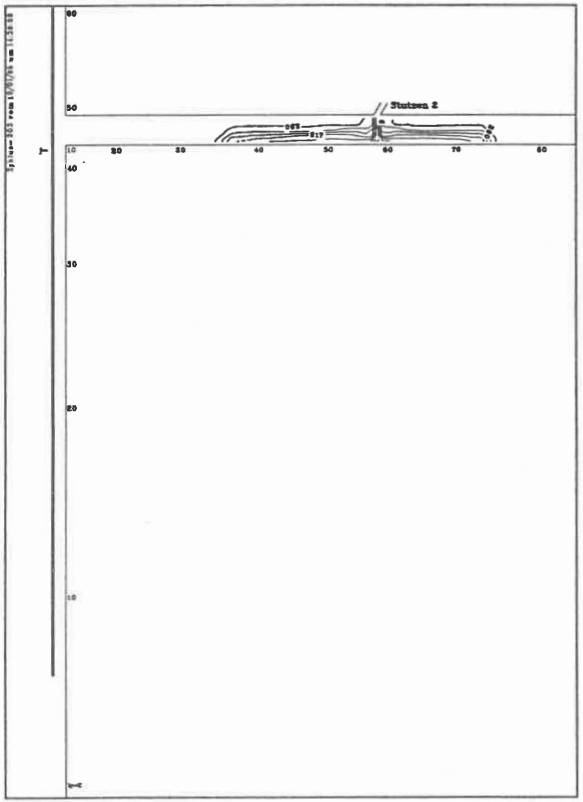

Fig. 3: Cold Leg Temperature

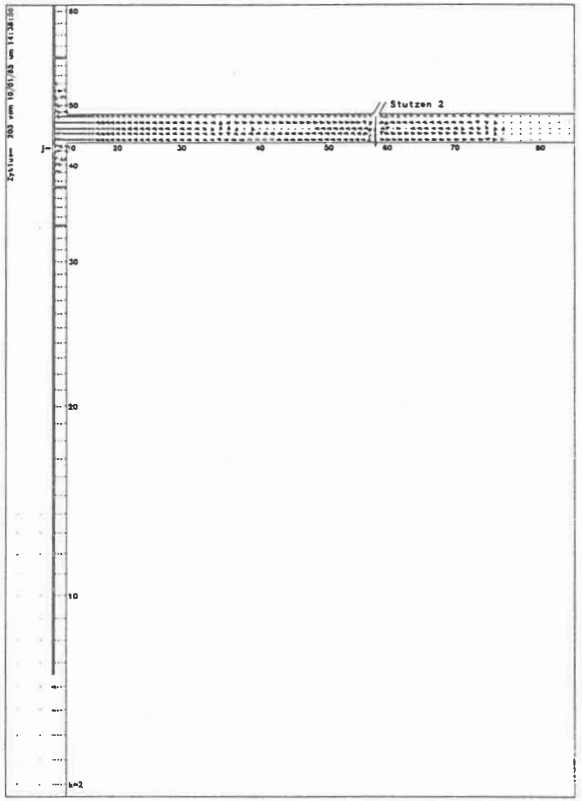

Fig. 4: Cold Leg Velocity

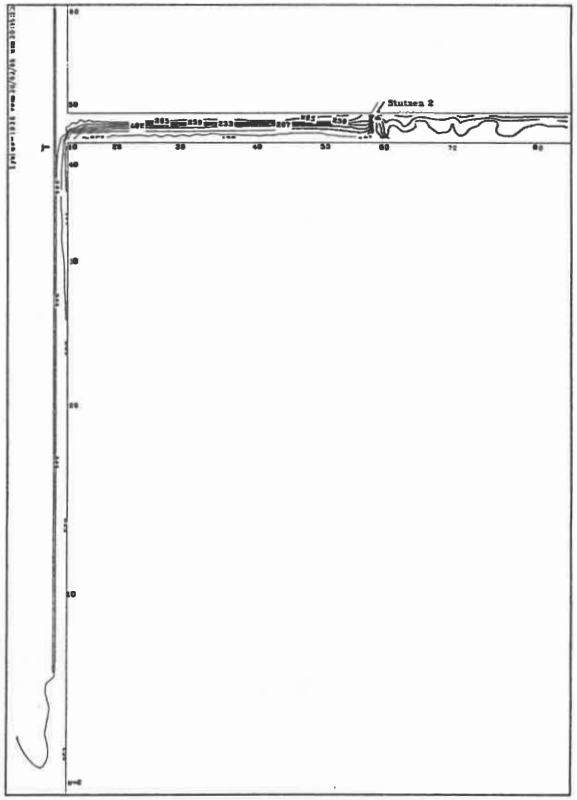

Fig. 5: Cold Leg Temperature

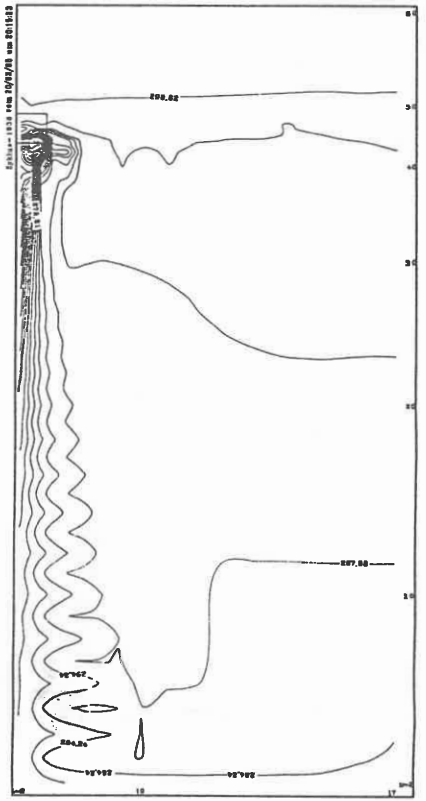

Fig. 6: Down Comer Temperature

Measurement and SOLA-PTS Calculations During the First 100 sec of Injection

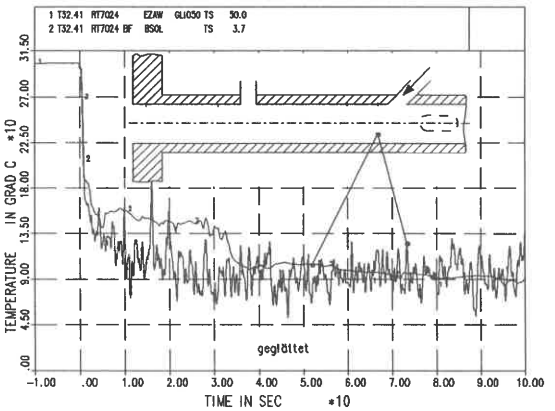

Fig. 7: Injection Area (Cold Leg)

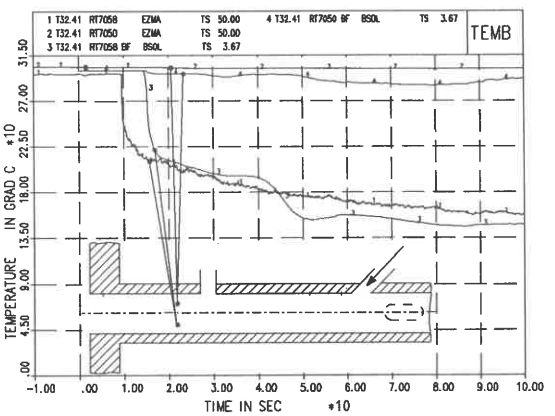

Fig. 8: Stratification in the Cold Leg

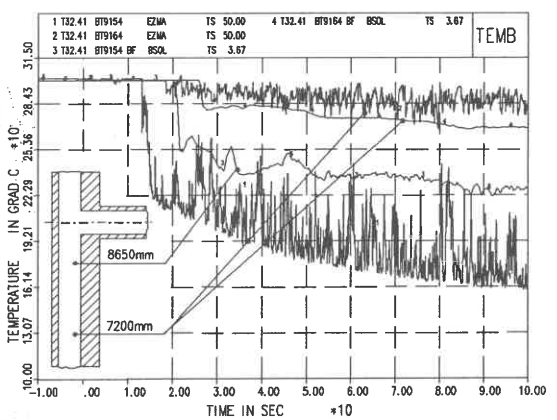

Fig. 9: Downcomer Area

Measured and SOLA-PTS Calculated Temperature Distribution in the Downcomer at t = 60 sec

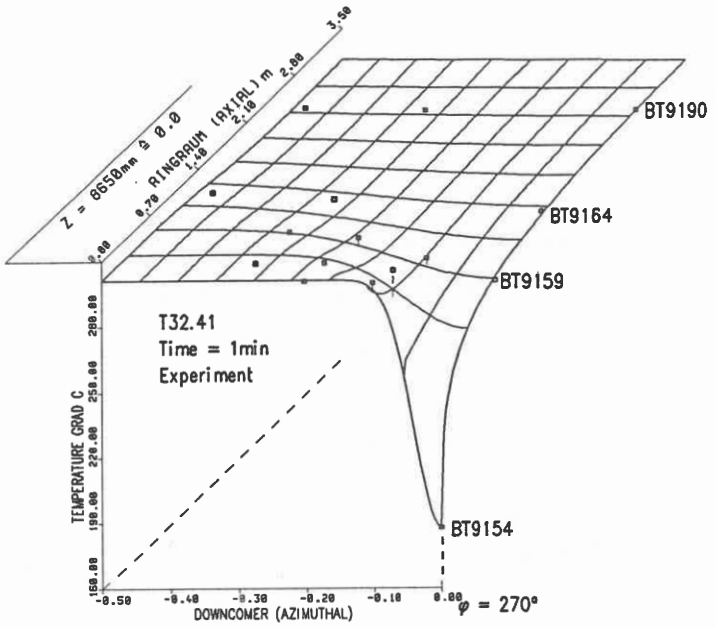

Fig. 10: Measured Distribution

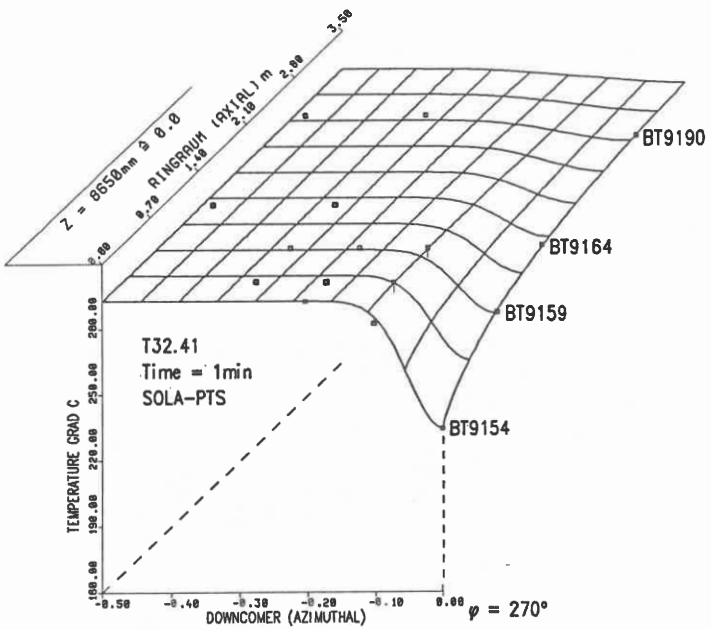

Fig. 11: SOLA-PTS Calculation

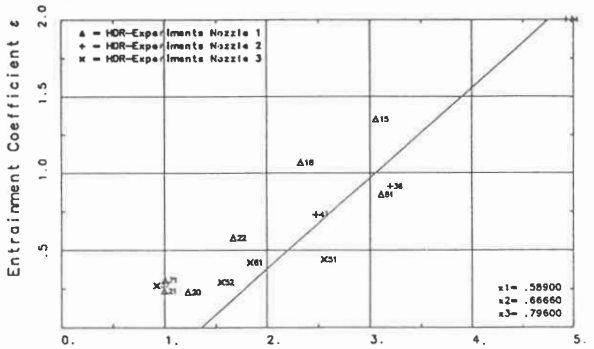

Fig. 12: Dimensionless Parameter η_{oh}
Comparison between Data and Correlation from Sun-Oh

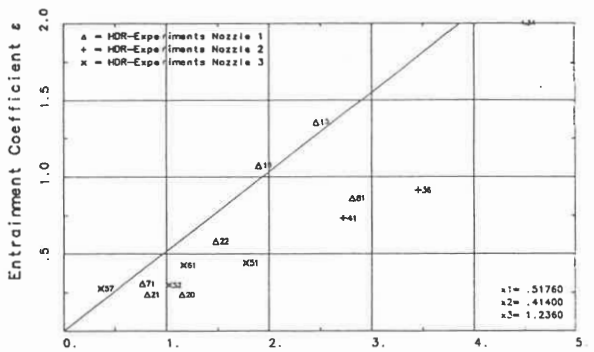

Fig. 13: Dimensionless Parameter η_{theo}
Comparison between Data and Correlation from Theofanous

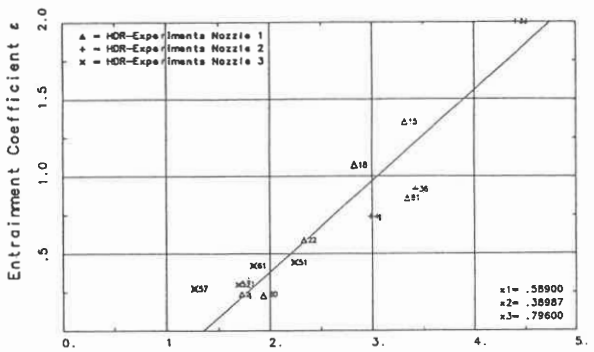

Fig. 14: Dimensionless Parameter η_{mod}
Modified Correlation for the Injection Area Entrainment

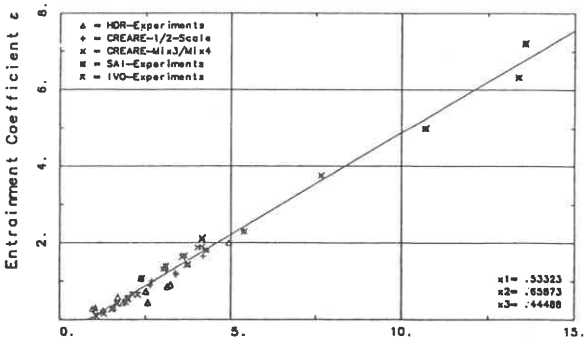

Fig. 15: Dimensionless Parameter η_{mod}
Modified Correlation for the Injection Area Entrainment

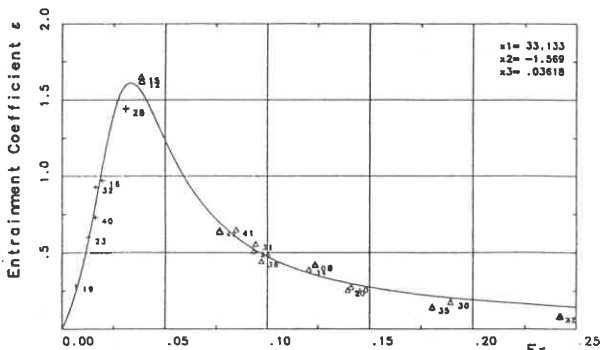

Fig. 16: Global Froude Number
Entrainment in the Injection Area – IVO Experiments

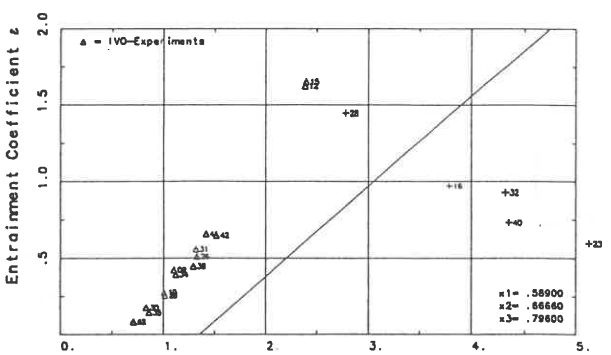

Fig. 17: Dimensionless Parameter η_{oh}
Comparison between Data and Correlation from Sun-Oh